Journal of Zhejiang University-SCIENCE A (Applied Physics & Engineering)
ISSN 1673-565X (Print); ISSN 1862-1775 (Online)
www.jzus.zju.edu.cn; www.springerlink.com
E-mail: jzus@zju.edu.cn

Seismic behaviour of an earthquake-resilient prefabricated beam-column cross joint*

Ai-lin ZHANG[1,3], Ying-xia WU[1], Zi-qin JIANG[†‡1,3], Xu-qiao ZHANG[2], Chao DOU[4]

([1]*College of Architecture and Civil Engineering, Beijing University of Technology, Beijing 100124, China*)

([2]*China State Construction Engineering Corporation, Beijing 100029, China*)

([3]*Beijing Engineering Research Center of High-rise and Large-span Prestressed Steel Structure, Beijing 100124, China*)

([4]*School of Civil Engineering, Beijing Jiaotong University, Beijing 100044, China*)

[†]E-mail: jzqbj2010@163.com

Received July 13, 2017; Revision accepted Aug. 13, 2017; Crosschecked Nov. 17, 2017

Abstract: Earthquake-resilient structures have become a hot topic in seismic research. Based on the concept of damage control, this paper presents a new type of earthquake-resilient prefabricated beam-column cross joint (ERPCJ). After a strong earthquake, the function of the joint can be quickly restored because damage is concentrated mainly on replaceable connecting parts. First, the construction and advantages of the ERPCJ are explained, and its seismic design requirements are established. Then, the theory behind the design of the ERPCJ is proposed and verified by numerical simulation using eight ERPCJ models. The hysteretic behaviour of the ERPCJ was investigated using the finite element (FE) method considering the effects of the weakening profile in the flange cover plate, the thickness and strength of the flange cover plate, the distance between the middle bolts, the gap between the beams, and the bolt hole shape. Finally, cyclic loading and repairing tests were conducted on a basic specimen, and the rationality of the design theory was verified. The seismic performance and the post-earthquake resilience performance of the joint were investigated. Numerical analysis and experiments showed that the proposed design theory could accurately predict the yield load of the ERPCJ. A reasonably well-designed ERPCJ should have good bearing capacity, collapse resistance capacity, seismic performance, and post-earthquake resilience performance. The thickness and strength of the flange cover plate, the distance between the middle bolts, and the gap between the beams have a large effect on the seismic behaviour of the joint, and so should be properly designed.

Key words: Earthquake-resilient; Flange cover plate; Weakening profile; Design theory; Hysteretic behaviour
http://dx.doi.org/10.1631/jzus.A1700358 **CLC number:** TV5

1 Introduction

Prefabricated steel structures have advantages such as standardization of design, feasibility of production in factories at different locations, and ease of assembly at the construction site. They can significantly reduce labour requirements and shorten the construction period. Prefabrication has become a new trend in the development of steel structures (Zhou *et al*., 2005; Zhang A.L. *et al*., 2014; 2016; 2017; Liu *et al*., 2015a; 2015b; Jiang *et al*., 2017a; 2017b). Such structures can be fully prefabricated to facilitate the installation and disassembly processes at the site. However, if the constitution and design of the prefabricated beam-column joint are not done correctly, the failure mode of the joint may be the same as that of bolt-welded joints, in which the global failure mode occurs mainly in the joint zone. This would

‡ Corresponding author

* Project supported by the National Key Basic Research and Development Program of China (No. 2016YFC0701504), the National Natural Science Foundation of China (No. 51608014), the Natural Science Foundation of Beijing, China (No. 8174060), and the China Postdoctoral Science Foundation (No. 2017T100020)

ORCID: Zi-qin JIANG, http://orcid.org/0000-0001-9613-3972

make the repair and reinforcement of prefabricated steel structures similar to that of traditional steel structures after an earthquake; thus, earthquake resilience would not be achieved. A properly constituted and designed prefabricated beam-column joint would enable the transfer of the failure that can occur in beams or columns to the replaceable parts. It would be necessary to replace only the damaged parts after an earthquake to recover the structure, and therefore the aseismic and earthquake resilience functions would be improved. Earthquake resilience has become an important topic in seismic research (Cimellaro *et al*., 2010; Lv *et al*., 2011; Zhang *et al*., 2013; Chen *et al*., 2016; Lu *et al*., 2016).

Many researchers have performed extensive studies on beam-column joints with cantilever beams. Plaud and Vogeltanz (1997) were the first to propose the concept of a dog-bone connection. Cutting a part of the beam flange at a certain distance from the beam end would make the plastic hinge shift away from welds, and ductile failure would occur in the joint. With numerical analyses and reversed cyclic loading on joints with all-bolt connections between concrete-filled square tubular steel columns and steel beams, Wu *et al*. (2005) proposed a method for calculation of the joint-panel stiffness, yield shear strength, and ultimate shear strength. Kim and Oh (2007) investigated the influence of the moment transferring effectiveness of the joint with a box-type column, and compared the results with those of a joint with an H-type column, through nonlinear finite element (FE) analyses of five joint models. Chen *et al*. (2006) conducted a hysteretic experiment on eight beam-column joints with crossing diaphragms and showed that this type of joint met the requirements of current seismic design codes. Di Sarno *et al*. (2003; 2006) considered the application of stainless steel to improve the response of the beam-to-column connections in steel moment resisting frames. Li *et al*. (2007) conducted a quasi-static experiment on three full-size cross-shaped specimens of diaphragm-through style beam-column joints under low reversed cyclic loading. The seismic performance of this type of joint was reported with respect to strength, deformation, and energy dissipation. Zhang Y.X. *et al*. (2014) evaluated the performance of joints with strengthened beam ends and weakened beam flanges through experimental and numerical studies. Their results showed that this joint could achieve shifting of the plastic hinge away from the weld, and thus the welds at the beam end could be protected. This type of joint also had good plastic rotation ability and energy dissipation ability. Jeddi *et al*. (2016) proposed a new through-rib stiffener beam connection, and tested four half-scale cruciform specimens. The results showed that the connection had a good ductility and energy dissipation capacity. El-Khoriby *et al*. (2017) established simplified FE models of steel beam-to-column connections under cyclic loading, and the FE analysis showed good agreement with experimental results for a cyclically loaded endplate connection. Further, the carrying capacity, initial stiffness, hysteretic behaviour, and energy dissipation capacity were compared and discussed.

In the field of earthquake resilience, Oh *et al*. (2009) installed a metallic slit damper on a beam-column joint to protect beams and columns, thus the plastic deformation was concentrated only at the slit dampers. Test results showed that the joint had a good seismic behaviour. Calado *et al*. (2013) conducted cyclic loading tests on 12 composite joints with a new fuse device. The results showed that the seismic behaviour of the joint was good, and it could prevent plastic deformation occurring on beams and columns. The main structure could be repaired by replacing a fuse device after an earthquake. Lv *et al*. (2016) introduced a replaceable coupling beam application to a reinforced concrete structure, and performed dynamic analysis of the entire structure. The results, which were validated through an ambient vibration test, indicated that the replaceable coupling beam had good seismic performance, which was achieved by concentrating the damage in the replaceable parts.

The traditional beam-column joints in cantilever beams normally use two flange cover plates for the connections, and stiffener plates are fixed on the beam ends to shift the plastic hinge away from the welds. However, this arrangement leads to a complicated stress field because of multiple welds, and makes it difficult to recover the structure after an earthquake. Thus, this paper presents a new type of earthquake-resilient prefabricated beam-column cross joint (ERPCJ) (Fig. 1). With a reasonably good design, the ERPCJ can shift the location of plastic deformation to the replaceable parts, and thus protect the main members in the elastic state. The function can be

recovered by replacing the plastic plates and bolts and then meet earthquake resilience requirements.

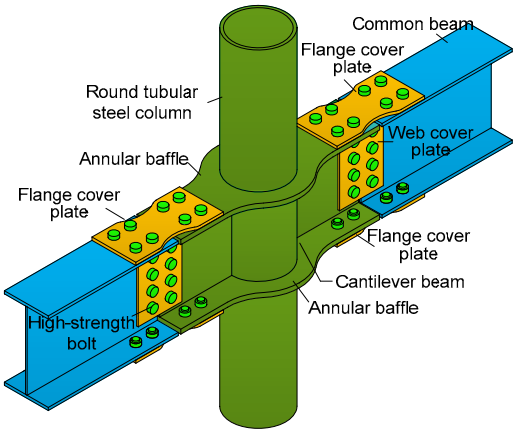

Fig. 1 Earthquake-resilient prefabricated beam-column cross joint (ERPCJ)

In this paper, we first elaborate the construction and advantages of the ERPCJ, and establish its seismic design requirements. Then, the theory behind the design of the ERPCJ is proposed and verified by numerical simulation using eight ERPCJ models. The hysteretic behaviour of the ERPCJ was investigated using the FE method. Finally, cyclic loading and repairing tests were conducted on a basic specimen, and the rationality of the design theory was verified. The seismic performance and the post-earthquake resilience performance of the joint were investigated.

2 Constitution, advantages, and seismic design requirements of ERPCJ

2.1 Constitution and advantages of ERPCJ

The ERPCJ consists of a round tubular steel column with cantilever beams, common beams, and replaceable connecting parts. Round tubular steel columns with cantilever beams and common beams can be manufactured in factories and quickly installed at the construction site by connecting the flanges and webs with cover plates and high-strength bolts (Fig. 2). This design has the following advantages and features which facilitate factory production and ease of assembly at the construction site:

1. The single cover plate connection makes the lower flange cover plate as a support for the common beams, thus making the installation more convenient at the construction site.

2. Only thickening the annular baffle and adjusting the weakening profile on the flange cover plate can transfer the plastic hinge to the outside of the joint, and to the replaceable connecting parts.

3. The joint can dissipate energy through plastic deformation and friction sliding of the cover plates. It can ensure that little damage occurs in columns and beams thus only need to replace replaceable connecting parts after an earthquake to recover the structure.

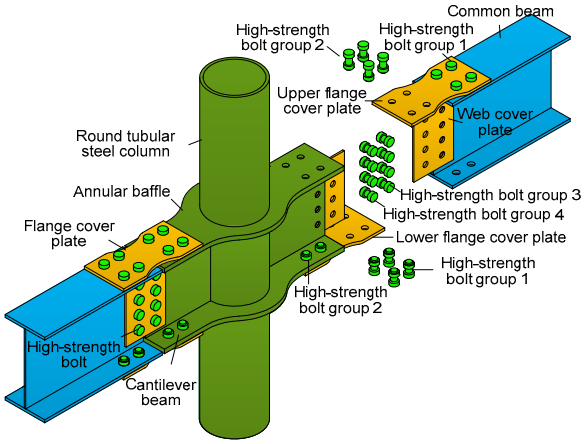

Fig. 2 Assembly details of the ERPCJ

2.2 Seismic design requirements of the ERPCJ

The ERPCJ should meet the following design requirements:

1. The common beam parts of the ERPCJ should not slide in normal service conditions. It implies that the shear bearing capacity of bolts should be larger than the axial force on the flange cover plate of ERPCJ under small earthquakes. This concept can be used to design bolts of the ERPCJ (Zhang *et al.*, 2017).

2. There shall be no damage to the ERPCJ under small earthquakes. This implies that the yield load P_y of the ERPCJ should be slightly greater than the yield load of the common beam over the whole span, P_{sby}. At this moment, the prefabricated beam-column cross joints should be in the elastic state.

3. The ERPCJ should not collapse under strong earthquakes. It means the joint shall still have good

bearing capacity even when the rotation of the joint is 0.02 rad (SAC, 2003). Besides, the ratio of the beam end load P to the ultimate bearing capacity of the ERPCJ (P_{max}) should always be greater than 0.8.

4. Plastic damage of the ERPCJ should be concentrated mainly on replaceable parts, not only when the load at beam end P reaches its ultimate capacity P_{max}, but also when the angle of rotation θ of the ERPCJ reaches 0.02 rad. Thus, all main members will remain in the elastic state. Only the damaged parts would need to be replaced after an earthquake, thereby improving the earthquake resilience function.

3 Design theory of ERPCJ

The design of the flange cover plate directly influences whether the ERPCJ can meet the seismic design requirements (Zhang *et al.*, 2017).

As the flange cover plate works for the overall bending of the combined section, its stress should satisfy the requirement of Eq. (1):

$$\sigma_{zt}=\frac{P_{sby}L_{sb}}{\chi_1 I_{cov}}\left(h_b/2+t_{cov,f}\right)\le f_{cov,y}, \tag{1}$$

where L_{sb} and h_b are the length and height of the common beam, respectively (Fig. 3); I_{cov} is the inertia moment of combined section A, discarding the influence of the web cover plate; χ_1 is the stiffness correction factor for section A, equal to 1.2, which considers the influence of the bolts binding effects; $t_{cov,f}$ and $f_{cov,y}$ are the thickness and yield strength of the cover plate, respectively.

Besides, compression flange cover plates should meet the stability bearing requirement as

$$\sigma_{jb}=\frac{N_{cov,y}}{\varphi_{cov}A_{cov}}\le f_{cov,y}, \tag{2}$$

where φ_{cov} and A_{cov} are the stability coefficient (SAC, 2003) and the area of the flange cover plate, respectively. $N_{cov,y}$ is the axial force on the flange cover plate which can be calculated by

$$N_{cov,y}=\frac{\eta_1 P_{sby}L_{sb}}{h_b+t_{cov,f}}, \tag{3}$$

where η_1 is the distribution coefficient of the section moment, equal to 0.9.

If σ_{zt} and σ_{jb} are small, the common beam may damage before the cover plate. Thus, the larger value between σ_{zt} and σ_{jb} should be close to $f_{cov,y}$; in other words, the requirement of Eq. (4) should be met:

$$0.9f_{cov,y}\le\max(\sigma_{zt},\sigma_{jb})\le f_{cov,y}. \tag{4}$$

Once $t_{cov,f}$ is determined, the yield load P_y can be obtained in the same way, which is given by

$$P_y=\min\left(\frac{\varphi_{cov}A_{cov}\left(h_b+t_{cov,f}\right)}{\eta_1 L_{sb}}f_{cov,y},\ \frac{\chi_1 I_{cov}}{\left(h_b/2+t_{cov,f}\right)L_{sb}}f_{cov,y}\right). \tag{5}$$

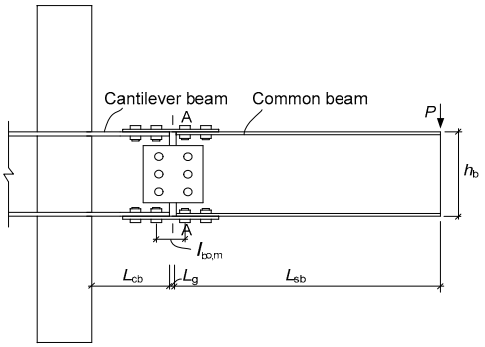

Fig. 3 Schematic diagram of the ERPCJ
L_{cb} is the length of the cantilever beam, $l_{bo,m}$ is the middle bolts distance, and L_g is the gap between the beams

4 Finite element model

Eight ERPCJs were designed to study the effects of the weakening profile in the flange cover plate, the thickness ($t_{cov,f}$) and strength of the flange cover plate, the middle bolts distance $l_{bo,m}$, the gap between the beams L_g, and the bolt hole shape on the energy dissipation capacity and hysteretic behaviour of the ERPCJ. The ERPCJs were classified into four groups. The round tubular steel column was a pipe with dimensions 377 mm×16 mm. The section of the joint zone was a pipe with dimensions 377 mm ×20 mm. The section of the common beam was 300 mm× 200 mm×6 mm×12 mm. To meet the requirements of

earthquake resilience, the cantilever beam section was strengthened with a section of 300 mm× 200 mm×12 mm×20 mm. The length of the column, the length of the cantilever beam L_{cb}, and the length of the common beam L_{sb} were 3000 mm, 512 mm, and 1400 mm, respectively. Three types of flange cover plates (Fig. 4) were considered in this study: a plate without weakening, a plate weakened by a circular arc type dog-bone profile, and a plate weakened by a straight dog-bone profile. These three types are marked as X1, X2, and X3, respectively. The code K1 in the name of a member indicates that the bolt holes on the common beam and the bolt hole in the middle of the cantilever beam web are circular, while the other holes in the cantilever beam are long and tapered (Fig. 5). K2 indicates that the bolt holes on the cantilever beam and the common beam are circular. The other related parameters of the joints are listed in Table 1. Among the various models, type SJ3 is the basic specimen designed using the theory proposed in this paper. Its geometry and other details are shown in Fig. 5.

The eight models of ERPCJs described above were modelled using ABAQUS (Fig. 6). All the members were modelled using solid elements C3D8R. The elastic modulus is 206 GPa. The yield strength of the flange cover plate and other steel plates are 235 MPa and 345 MPa, respectively, with the hardening module of 2% elastic modulus (Jiang *et al*., 2015; 2017a; Zhang *et al.*, 2017). Each member was divided into two units in the thickness direction, and there were about 290000 units. The contact

Table 1 Parameters of specimens

Model	$t_{cov,f}$ (mm)	L_g (mm)	$l_{bo,m}$ (mm)	Material of flange cover plate
X1-K1-SJ1	16	20	320	Q235B
X2-K1-SJ2	16	20	320	Q235B
X3-K1-SJ3	16	20	320	Q235B
X3-K1-SJ4	12	20	320	Q235B
X3-K1-SJ5	16	20	320	Q345B
X3-K1-SJ6	16	20	160	Q235B
X3-K1-SJ7	16	6	320	Q235B
X3-K2-SJ8	16	20	320	Q235B

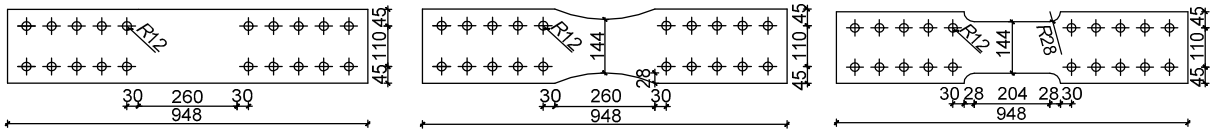

Fig. 4 Schematic diagrams of flange cover plates SJ1–SJ3 (unit: mm)

(a) Flange cover plate without weakening; (b) Flange cover plate weakened by a circular arc type dog-bone profile; (c) Flange cover plate weakened by a straight dog-bone profile

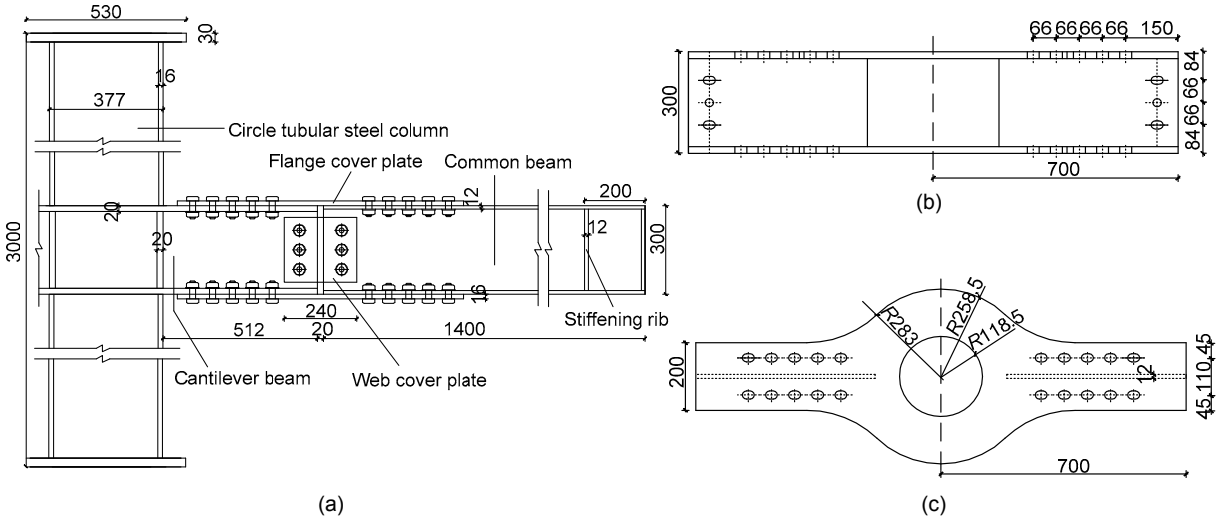

Fig. 5 Geometry of basic specimen SJ3 (unit: mm)

(a) Geometry of the specimen; (b) Front view of the cantilever beam; (c) Top view of the cantilever beam

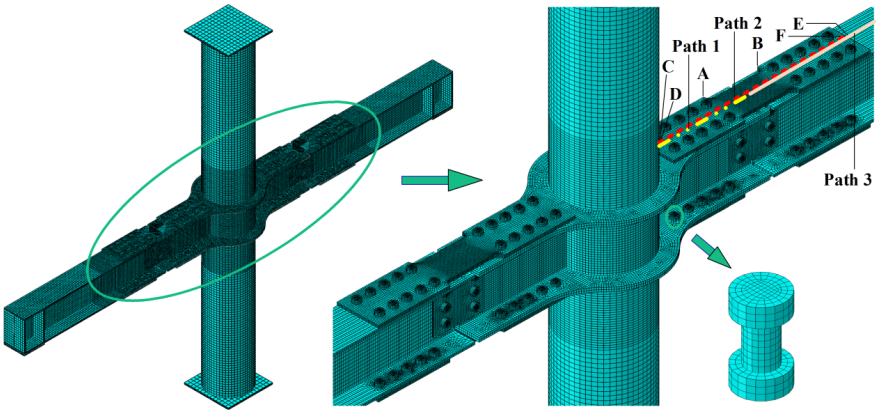

Fig. 6 Finite element model

relationships were set between the cantilever beam and the flange cover plate and bolts, and between the common beams and the flange cover plate and bolts. A tie constraint was provided between the cantilever beam and the steel columns. Grade 10.9 high-strength friction bolts were used in these specimens, and the pretension force was set as 190 kN. A friction coefficient of 0.45 was considered on the interfaces between the plates (SAC, 2003). A rigid body condition was set at the end of the steel columns. The hinged boundary condition was set at the central point of the rigid body, and the axial compression ratio applied on the end column was 0.3. The out-of-plane deformations of the beams were constrained in the analysis. Anti-symmetric displacement constraint was set on both sides of the common beam ends to simulate the loading on the ERPCJ. The loading law is shown in Fig. 7. To observe the deformation at the key points and the stress distribution in each member, the observation points and the stress distribution paths were numbered (Fig. 6). Among them were the following key observation points: point *A*, at the dog-bone profile section on the flange cover plate, close to the cantilever beam side; point *B*, at the dog-bone profile section on the flange cover plate, close to the common beam side; point *C*, at the end of the flange cover plate, close to the cantilever beam side; point *D*, on the cantilever beam, its position corresponding to the position of point *C*; point *E*, at the end of the flange cover plate, close to the common beam side; point *F*, on the common beam, its position corresponding to the position of point *E*. Path 1 was the longitudinal mid-line on the upper face of the upper flange of the

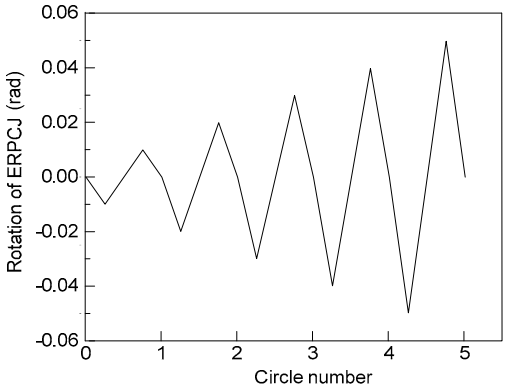

Fig. 7 Displacement loading law

cantilever beam. Path 2 was the longitudinal mid-line on the lower face of the upper flange cover plate. Path 3 was the longitudinal mid-line on the upper face of the upper flange of the common beam (Zhang *et al.*, 2017).

5 Results of numerical analysis

5.1 Yield load

Fig. 8 shows the design load, theoretical yield load, and numerical results of the yield load for all ERPCJ models. The theoretical yield load was calculated using Eq. (5). The design load is the yield load of the common beam over the whole span, P_{sby}. The figure shows that the yield load of the ERPCJ obtained by FE analysis of each specimen is in good agreement with the theoretical value: the deviation is within 5%, which proves the accuracy of the design

theory. There was a large difference between the yield load and the design load P_{sby} of SJ1, SJ4, and SJ5, which is in contradiction with the seismic design requirements of the joint, explained in Section 2.1. Note that although the yield load of SJ6 coincides with the design load P_{sby}, the ultimate bearing capacity is high because of the short distance between the middle bolts; thus, the beam and the column become partly plastic, and would not meet the requirements for earthquake resilience.

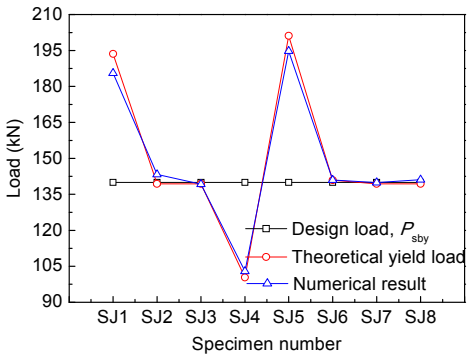

Fig. 8 Verification of the design theory

5.2 Hysteretic behaviour

Fig. 9 shows the hysteretic loop of each ERPCJ. The loops are large and have no significant pinch phenomena. The areas inside the hysteretic loops are large and of good symmetry, which indicates good energy dissipation capacity. Most of the plastic deformation of the joints was concentrated on the flange cover plates, which shows good ductility. Moreover, the ductility of the joints could be improved further by the sliding of the bolts.

From the comparison of the hysteretic loops of SJ1–SJ3 (Fig. 9a), the effect of the flange cover plate with weakened form on the hysteretic behaviour of the joints can be studied. Compared with the basic specimen SJ3, SJ1 had no weakening effect on the flange cover plates, and the bending stiffness of the connection was larger, which improved the initial stiffness and ultimate bearing capacity of the joint. However, as the flange cover plate was not weakened, plasticity developed mainly around the bolt holes, which made it difficult to realize the damage control of the joint. In SJ2, the flange cover plate was

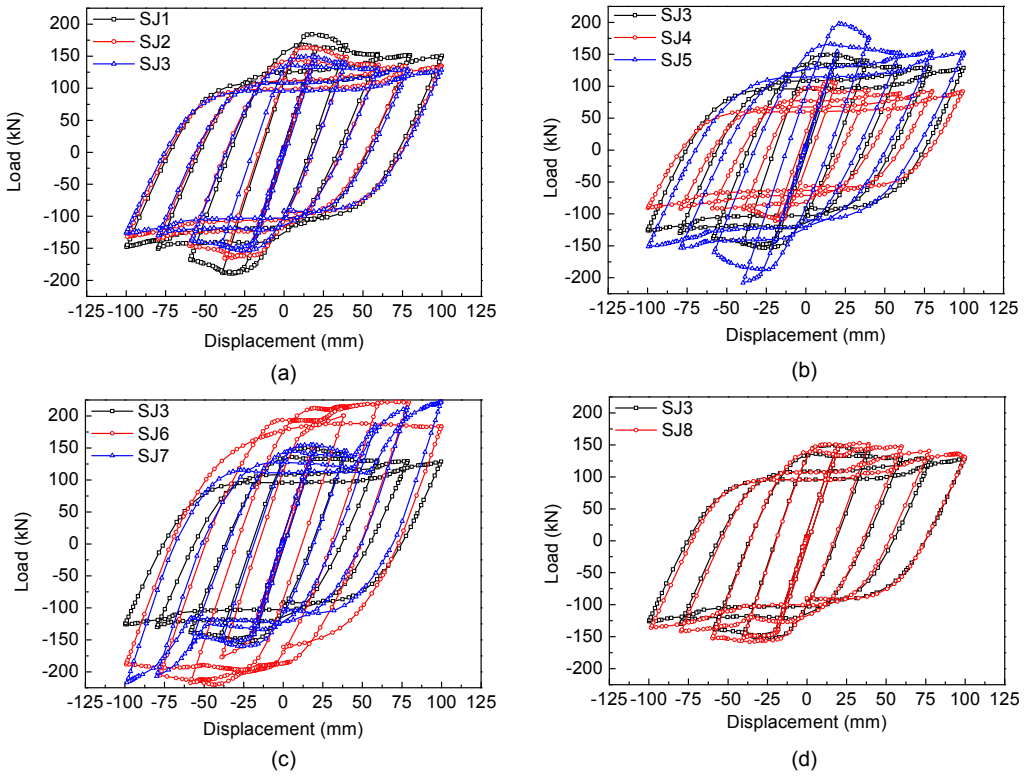

Fig. 9 Hysteretic loops

(a) Specimens SJ1, SJ2, SJ3; (b) Specimens SJ3, SJ4, SJ5; (c) Specimens SJ3, SJ6, SJ7; (d) Specimens SJ3, SJ8

weakened by a circular arc type dog-bone profile, and its weakened area was about the same as that in SJ3, so the hysteresis loop of SJ2 broadly matched that of SJ3. The small difference observed was because the bending stiffness of the flange cover plate weakened by a circular arc type dog-bone profile was slightly larger than that of the flange cover plate weakened by a straight dog-bone profile. Thus, weakening by dog-bone profile was found to be suitable for controlling the plastic damage of the beam-column joint. Weakening by the straight dog-bone profile was more suitable for establishing the design theory.

From the comparison of the hysteretic loops of SJ3–SJ5 (Fig. 9b), the effect of the thickness and strength of the flange cover plates on the hysteretic behaviour of the joint could be studied. The flange cover plate of SJ4 was thin, the initial stiffness of the joint was low, and hence the yield load of the joint, P_y, was lower than the design load P_{sby}, which is against the seismic design requirement. The flange cover plate of SJ5 was made of Q345B material. Though the initial stiffness of SJ5 was the same as that of SJ3, the yield load and ultimate bearing capacity of SJ5 were significantly higher than those of SJ3. In particular, the ultimate bearing capacity of SJ5 was much higher than the design load, which made it difficult to maintain the beam and the column in the designed elastic state.

Fig. 9c shows a comparison of the hysteretic loops of SJ3, SJ6, and SJ7. Reducing the distance between the middle bolts, $l_{bo,m}$, of SJ6 improved the initial stiffness of the joint to a certain extent without influencing the yield load of the joint. The ultimate bearing capacity of SJ6 was significantly higher than that of SJ3, as expected from theory. As the gap L_g of SJ7 was smaller, when the rotation of the joint reached 0.22 rad, collision occurred between the cantilever beam and the common beam, and the bearing capacity of the joint increased rapidly. Hence, stress concentration occurred in the contact position of the cantilever beam and the common beam, resulting in the yielding of the main members.

Fig. 9d shows the influence of the bolt hole shapes on the hysteretic behaviour of the joints. The long tapered hole on basic specimen SJ3 can not only allow the common beam to rotate around the circular holes on the cantilever beam web, but also help avoid stress concentration caused by extrusion between the bolts and the hole walls, and realize sliding of the bolts to dissipate energy. Because of the circular holes on the cantilever beam of SJ8, there is little slippage of the bolts. With increasing loading displacement, the bolts start making contact with the hole walls, then the bearing capacity of the specimen increases slightly, and the stress concentration around the hole walls becomes significant.

Fig. 10 shows the load-displacement curve of the cantilever beam end of the four representative ERPCJs. The hysteretic loops of specimens SJ1 and SJ3 are linear, which implies that the cantilever beams of SJ1 and SJ3 are in the elastic state. However, the related curves of SJ6 and SJ7 are fusiform, and there is residual deformation on the cantilever beam at the loading end. This shows that the cantilever beams of SJ6 and SJ7 reach a plastic state gradually during the loading process, which goes against the requirement of earthquake resilience.

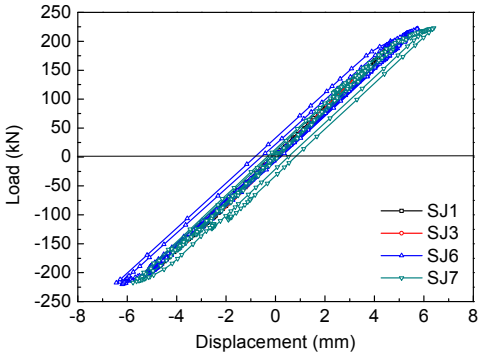

Fig. 10 Load-displacement curve of cantilever beam end

5.3 Failure mode

Fig. 11 shows the failure modes and von Mises stresses (for a rotation of 0.05 rad) of the four representative ERPCJs. All the flange cover plates of each joint buckle, and plastic deformation is concentrated mainly on the flange cover plates. Compared with SJ3, the plastic zone occurs locally on the web in SJ1. In SJ6, it develops locally on the innermost bolt hole of the cantilever beam and the outermost bolt hole of the common beam, and develops over a wide area on the flange cover plate, making it vulnerable to fracture. In SJ7, because of the small gap L_g, collision occurs between the cantilever beam and the common beam, which causes the plastic zone to occur locally on the cantilever beam end. On the whole, SJ3 shows

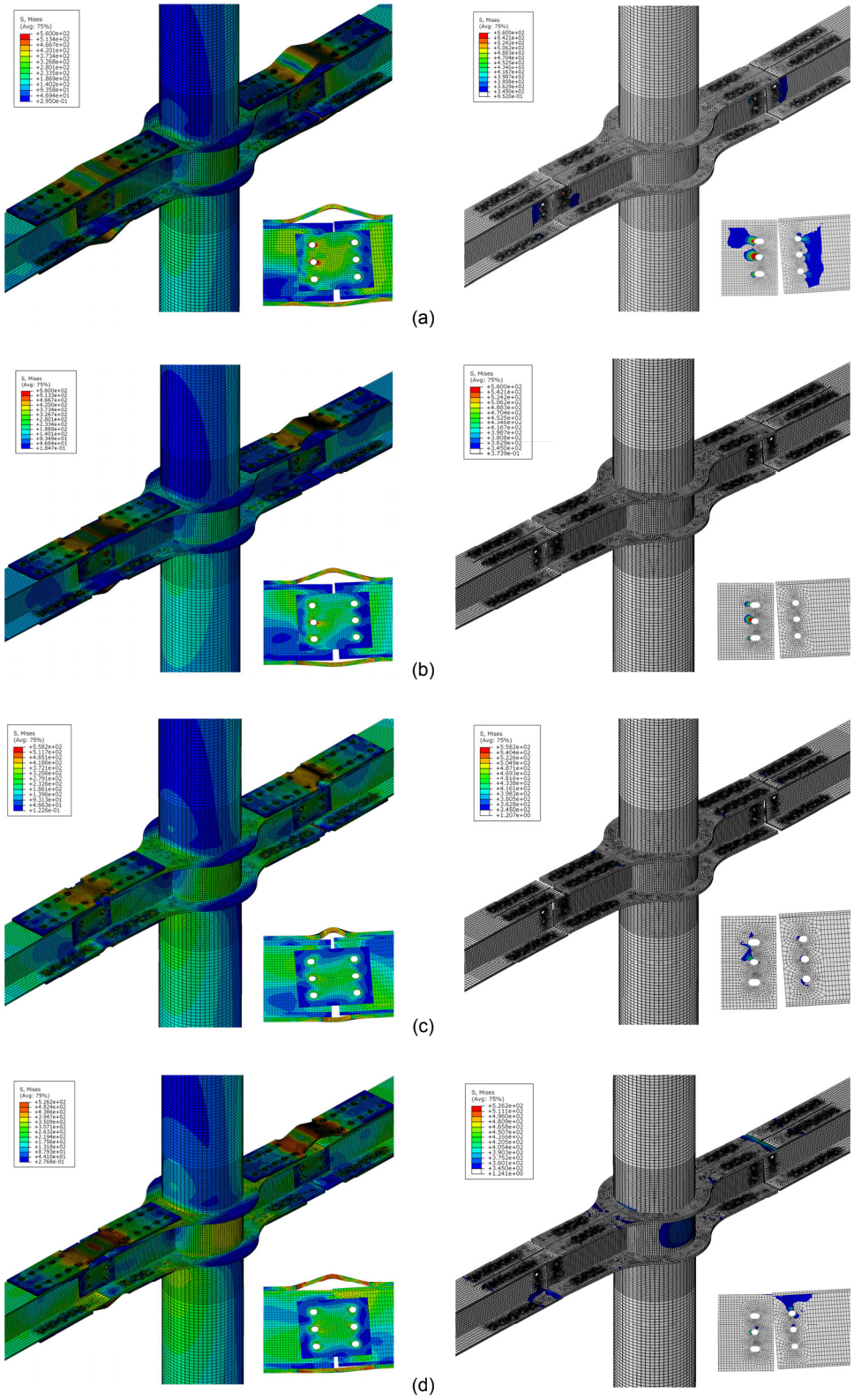

Fig. 11 FE analysis results (at 0.05 rad) of failure mode and von Mises stress on specimen: (a) SJ1; (b) SJ3; (c) SJ6; (d) SJ7. The figures on the left show the failure mode and von Mises stress, and those on the right show the plastic zones (the color areas represent the areas where the von Mises stress exceeds the yield stress). Note: for interpretation of the references to color in this figure legend, the reader is referred to the web version of this article

good earthquake-resilient behaviour. Its beam and column are in the elastic stage when the rotation of ERPCJ is 0.05 rad. It is necessary to replace only the connection members and high strength bolts; thus, it meets the requirements of earthquake resilience.

5.4 Stress distribution

Fig. 12 shows the stress distributions (at a rotation of 0.05 rad) of the four representative ERPCJs. The zero point on the horizontal axis represents the intersection point of the column central line and the upper surface of the upper flange of the cantilever beam. The stress distributions on the upper flange of the cantilever beam, the upper flange cover plate, and the upper flange of the common beam, along the direction of the members are shown. Fig. 6 shows the paths of the stresses. Fig. 12 shows that the high-stress region is concentrated on the flange cover plate. Because of the large moment at the cantilever beam end, the stress in this position is also large. In the flange cover plate, the first row of bolts on the common beam shows stress concentration phenomenon, and the stress in the remaining bolts is low. The maximum stress occurs in the position weakened by the dog-bone profile on the upper flange cover plate. The stress concentration phenomenon is significant, and the plastic deformation is large, which leads to failure of the joint. The figure shows that there is large variation in the stress distribution on the flange cover plate. This is due to the instability and buckling of the flange cover plate, and the inflection point that occurs on the flange cover plate.

Compared with the basic specimen SJ3, the stiffness of the flange cover plate of SJ1 is larger, so the bearing capacity of SJ1 is higher, which causes slightly higher stresses around the upper flange bolt holes of the common beam. The distance between the middle bolts of SJ6 is small, which makes the flange cover plate difficult to buckle. The ultimate bearing capacity of SJ6 is much greater than its yield load, leading to high stresses on the cantilever beam and plasticity occurring partly in the common beam. A small gap L_g is set between the cantilever beam and the common beam of SJ7, thus extrusion contact occurs between the cantilever beam and the common beam at the loading end, and the stress at the contact

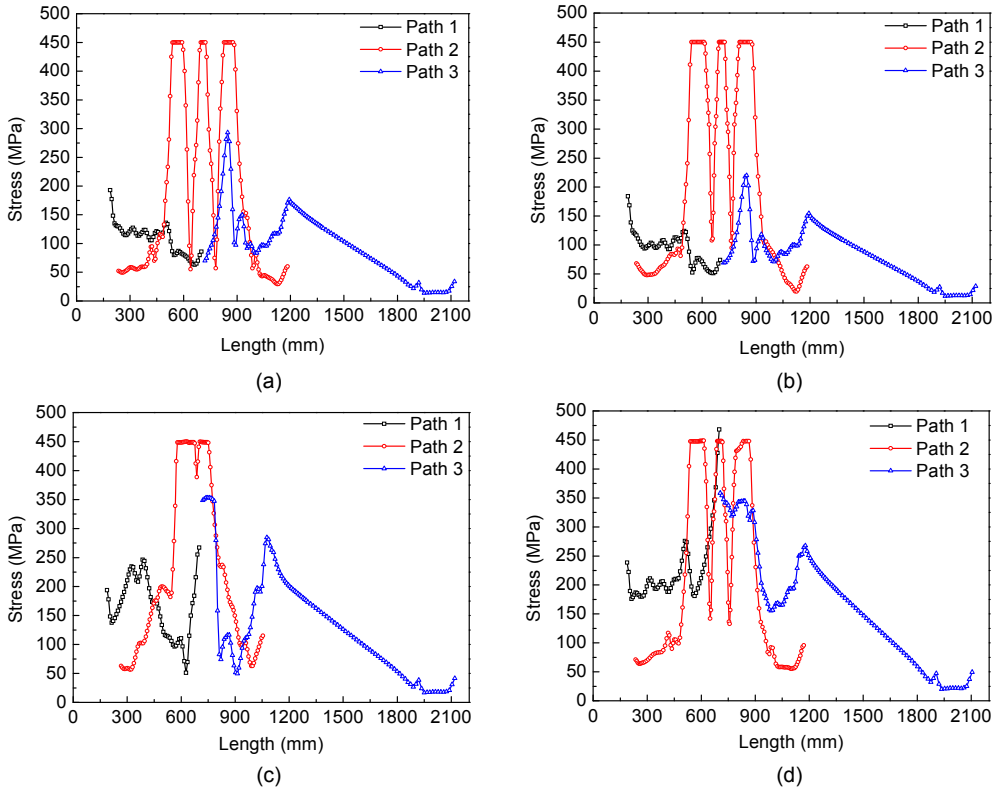

Fig. 12 Stress distributions on the cantilever beam, flange cover plate and upper flange of the common beam
(a) Specimen SJ1; (a) Specimen SJ3; (a) Specimen SJ6; (a) Specimen SJ7

position increases significantly. Furthermore, the stress at both sides is higher than the yield stress of 345 MPa. Thus, both sides reach the plastic stage, and hence do not satisfy the requirements of an earthquake-resilient joint. Compared with the other specimens, the stresses on the cantilever beam and the common beam of SJ3 are small. There is almost no damage in SJ3, and plastic deformation is concentrated mainly on the flange cover plate. Thus, replacing the connection members and high strength bolts after an earthquake is feasible, and the requirements of earthquake resilience can be met.

5.5 Relative displacement

Fig. 13 shows the relative displacement of point *A* and point *B* at the dog-bone profile section on the flange cover plate of the three representative ERPCJs. With cyclic loading, the upper and lower flange cover plates bear the circulation of tensile and pressure, respectively. The larger the relative displacement of point *A* and point *B*, the greater is the plastic deformation of the flange cover plate. Compared with SJ3, the distance between the middle bolts $l_{bo,m}$ of SJ6 is small, which makes the flange cover plate difficult to buckle, so the initial relative displacement of the two key points at the dog-bone profile section on the flange cover plate is small. With the gradual increase of the bearing capacity, the relative displacement also increases and the degree of plastic deformation of the flange cover plate is large. A small gap L_g is set between the cantilever beam and the common beam of SJ7. Thus, the compressive deformation of the cover plate is limited, resulting in the small relative displacement of the two key points (points *A* and *B*) at the dog-bone profile section on the flange cover plate and the small plastic deformation of the flange cover plate.

Appropriate sliding action of the flange cover plate will increase the ductility of the ERPCJ. Fig. 14 gives the relative sliding displacement curve of key points on the cantilever beam and the common beam to the flange cover plate end. The sliding action of the flange cover plate in SJ3 and SJ7 is stable, which can increase the ductility of the joint. The sliding action of the flange cover plate of SJ6 is large, so that the ductility of the joint is good. However, the bearing capacity of SJ6 is high, which makes it difficult to maintain the beam and the column in the designed elastic state.

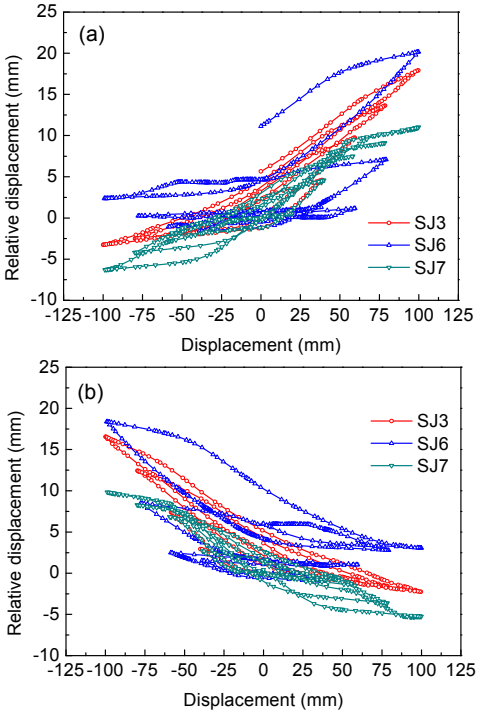

Fig. 13 Relative displacement of point *A* and point *B* at the dog-bone profile section on the flange cover plate: (a) upper and (b) lower flange cover plates of specimens SJ3, SJ6, and SJ7

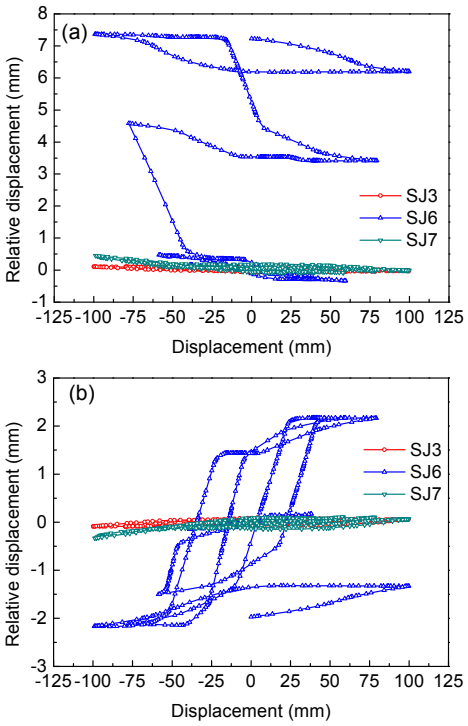

Fig. 14 Relative sliding displacement of key points *C*, *D* (a) and *E*, *F* (b)

6 Cyclic loading test

6.1 Test programme

To verify the design theory and seismic performance of the ERPCJ, cyclic loading and repairing tests were conducted on a well-designed specimen (SJ3) referred to in Section 4. The material properties of the steel plate were tested according to the requirements of GB/T 228.1-2010 (SAC, 2010). The results are presented in Table 2.

The tests were conducted in the Engineering Structural Test Centre of Beijing University of Technology, China. The loading system is shown in Fig. 15. The top and the bottom of the circular steel column were hinged. Axial force was applied on the top end of the column, and the axial compression ratio was 0.3. At the ends of both sides of the steel beams, hydraulic jacks were set to apply the cyclic load. At the end of the beam, a lateral brace was set to prevent out-of-plane deformation occurring on the beam. The loading law was made according to the American seismic code ANSI/AISC 341-10 (AISC, 2010) (Table 3).

Table 2 Material properties of steel plate

Member	Thickness (mm)	Yield strength, f_y (MPa)	Tensile strength, f_u (MPa)	f_u/f_y
Flange cover plate	16	254	391	1.54
Other plates	6	379	514	1.36
	12	368	526	1.43
	20	372	572	1.54

Fig. 15 Test loading system

Table 3 Test loading law

Load level	Rotation of joint (rad)	Cycle index	Maximum displacement at the beam end (mm)
1	0.00375	6	7.57
2	0.005	6	10.10
3	0.0075	6	15.15
4	0.01	4	20.20
5	0.015	2	30.30
6	0.02	2	40.40
7	0.03	2	60.59
8	0.04	2	80.78
9	0.05	2	100.96

6.2 Test results

Fig. 16 shows the hysteretic curve of the specimen. At the beginning of the loading (when joint rotation was not more than 0.01 rad) the load-displacement curve increased linearly in both the positive and negative directions, so the specimen was in the elastic stage. There was neither relative sliding between the cover plates nor significant deformation of the flange cover plates. When the specimen was loaded to the first loop of the fifth load level (when joint rotation was 0.015 rad), slight buckling deformation occurred on both sides in the weakened area of the compressed flange cover plate. At the same time, the peak point of the load-displacement curve occurred. As the loading continued, the deformation of the flange cover plate kept increasing, and the plastic area continued to expand along with the sliding action of the bolts. After the specimen was loaded to the ninth load level (when joint rotation was 0.05 rad), the test was completed. Significant deformation occurred in the flange cover plate (Fig. 17). During the entire test, no significant deformation was observed in the beam and column (Fig. 18).

By replacing the flange cover plate and the high strength bolts in the basic specimen, a repaired specimen was prepared. The above test was repeated on the repaired specimen using the same loading system and loading law. The results observed during this test were similar to those seen in the basic specimen. The plastic deformation of the flange cover plate and the global deformation of the joint at the end of the test are shown in Figs. 19 and 20, and the hysteretic curve of the repaired specimen is shown in Fig. 16.

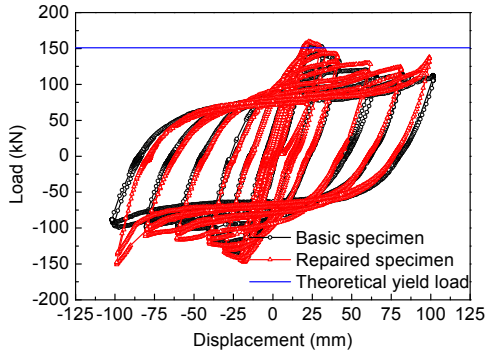

Fig. 16 Hysteretic curves

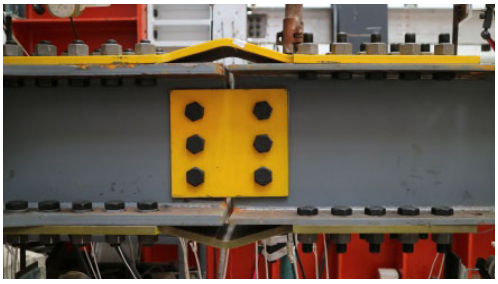

Fig. 17 Flange cover plate deformation of the basic specimen

Fig. 18 Deformation of the basic specimen

Fig. 19 Flange cover plate deformation of the repaired specimen

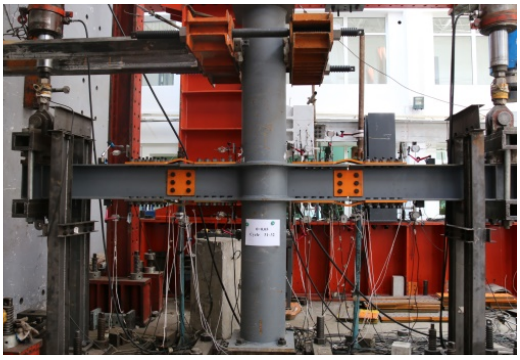

Fig. 20 Deformation of the repaired specimen

Fig. 16 shows that the yield load of the basic specimen was 132.3 kN, and that of the repaired specimen was 137.4 kN. The theoretical yield load obtained from Eq. (5) is 151.1 kN based on the material property test results. Considering that the test results might have been influenced by imperfections in the initial geometry and installation and the presence of residual stress, the difference of 10% between the test result and the theoretical value is acceptable, and it can be considered that the specimen meets the engineering requirements. When the joint rotation was 0.02 rad, the beam end load was about 0.86 times P_{max}, and when the joint rotation was 0.04 rad, the beam end capacity was still larger than 0.60 times P_{max}. This shows that the joint had a good bearing capacity and collapse resistance capacity. In addition, during the entire loading process, the main components such as beams and columns did not undergo significant deformation, and basically remained in the elastic state. The hysteretic curves of both the basic specimen and the repaired specimen were plump, and the shapes were the same, which implies that the joint had a good seismic performance and post-earthquake resilience performance. Thus, we conclude that the ERPCJ designed in this study can meet the requirements of bearing capacity and earthquake resilience.

7 Conclusions

In this paper, the constitution, advantages, and seismic design requirements of an ERPCJ were elaborated, and the theory behind its design was explained. Numerical simulation was conducted on eight ERPCJ models to verify the design theory and to

investigate the seismic behaviour of the ERPCJ. Finally, cyclic loading and repairing tests were conducted on the basic specimen. Based on the study, the following conclusions were drawn.

1. Numerical analyses showed that the proposed design theory could accurately predict the yield load of the ERPCJ. A well-designed ERPCJ can have a good bearing capacity and hysteretic behaviour. There would be almost no damage occurring in the cantilever beam and the common beam after an earthquake. Only the replaceable connecting parts need to be replaced after an earthquake to recover the structure.

2. If a straight dog-bone profile is used for weakening in the flange cover plate, the ductility of the joint would be improved and the bearing capacity could be ensured. The thickness and material properties of the flange cover plate directly influence the yield load of the ERPCJ. Therefore, the main parameter values should be selected strictly according to the design theory.

3. The short distance between the middle bolts had little influence on the yield load of the joint, but it made the flange cover plate difficult to buckle. This made the joint too strong to protect beams, and columns remained in the elastic state. If the gap between the beams is small, collision would occur between the cantilever beam and the common beam, which is against the requirements of earthquake resilience.

4. Experiments showed that the design theory could approximately predict the yield load of the specimen. Furthermore, the test results showed that the ERPCJ designed by the proposed theory had a good bearing capacity, collapse resistance capacity, seismic performance, and post-earthquake resilience performance, and could meet the requirements of earthquake resilience.

References

AISC (American Institute of Steel Construction), 2010. Seismic Provisions of Structural Steel Buildings, ANSI/AISC 341-310. AISC, Chicago, USA.

Calado, L., Proença, J.M., Espinha, M., *et al*., 2013. Hysteretic behaviour of dissipative bolted fuses for earthquake resistant steel frames. *Journal of Constructional Steel Research*, **85**(6):151-162. http://dx.doi.org/10.1016/j.jcsr.2013.02.016

Chen, Y.Y., Gang, L.I., Zhuang, L., *et al*., 2006. Experimental study on the seismic performance of diaphragm through type joint connecting H beam and tube column in steel frame. *Progress in Steel Building Structures*, **8**(1):23-30 (in Chinese).

Chen, Y.Y., He, X.Z., Ke, K., *et al*., 2016. Characteristics and technical issues on structural systems with replaceable damage-concentrated elements. *Journal of Building Structures*, **37**(2):1-10 (in Chinese).

Cimellaro, G.P., Reinhorn, A.M., Bruneau, M., 2010. Framework for analytical quantification of disaster resilience. *Engineering Structures*, **32**(11):3639-3649. http://dx.doi.org/10.1016/j.engstruct.2010.08.008

Di Sarno, L., Elnashai, A.S., Nethercot, D.A., 2003. Seismic performance assessment of stainless steel frames. *Journal of Constructional Steel Research*, **59**(10):1289-1319. http://dx.doi.org/10.1016/S0143-974X(03)00067-1

Di Sarno, L., Elnashai, A.S., Nethercot, D.A., 2006. Seismic retrofitting of framed structures with stainless steel. *Journal of Constructional Steel Research*, **62**(1):93-104. http://dx.doi.org/10.1016/j.jcsr.2005.05.007

El-Khoriby, S., Sakr, M.A., Khalifa, T.M., *et al*., 2017. Modelling and behaviour of beam-to-column connections under axial force and cyclic bending. *Journal of Constructional Steel Research*, **129**:171-184. http://dx.doi.org/10.1016/j.jcsr.2016.11.006

Jeddi, M.Z., Sulong, N.H.R., Khanouki, M.M.A., 2016. Seismic performance of a new through rib stiffener beam connection to concrete-filled steel tubular columns: an experimental study. *Engineering Structures*, **131**:477-491. http://dx.doi.org/10.1016/j.engstruct.2016.10.038

Jiang, Z.Q., Guo, Y.L., Tong, J.Z., *et al*., 2015. Design method of the pinned external integrated buckling restrained braces with extended core. Part II: finite element numerical verification. *Journal of Zhejiang University-SCIENCE A (Applied Physics & Engineering)*, **16**(10):793-804. http://dx.doi.org/10.1631/jzus.A1400325

Jiang, Z.Q., Guo, Y.L., Zhang, A.L., *et al*., 2017a. Experimental study of the pinned double rectangular tube assembled buckling-restrained brace. *Journal of Zhejiang University-SCIENCE A (Applied Physics & Engineering)*, **18**(1):20-32. http://dx.doi.org/10.1631/jzus.A1600483

Jiang, Z.Q., Dou, C., Guo, Y.L., *et al*., 2017b. Theoretical study on design methods for pinned assembled BRB with flat core. *Engineering Structures*, **133**:1-13. http://dx.doi.org/10.1016/j.engstruct.2016.12.004

Kim, Y.J., Oh, S.H., 2007. Effect of the moment transfer efficiency of a beam web on deformation capacity at box column-to-H beam connections. *Journal of Constructional Steel Research*, **63**(1):24-36. http://dx.doi.org/10.1016/j.jcsr.2006.02.009

Li, L.M., Chen, Z.H., Li, N., 2007. Experimental study on seismic capability of diaphragm-through style beam-column joint. *Journal of Earthquake Engineering & Engineering Vibration*, **27**(1):46-53 (in Chinese).

Liu, X.C., Xu, A.X., Zhang, A.L., *et al*., 2015a. Static and

seismic experiment for welded joints in modularized prefabricated steel structure. *Journal of Constructional Steel Research*, **112**(9):183-195. http://dx.doi.org/10.1016/j.jcsr.2015.05.003

Liu, X.C., Pu, S.H., Zhang, A.L., *et al*., 2015b. Static and seismic experiment for bolted-welded joint in modularized prefabricated steel structure. *Journal of Constructional Steel Research*, **115**(12):417-433. http://dx.doi.org/10.1016/j.jcsr.2015.08.036

Lu, X., Chen, C., Chen, Y., *et al*., 2016. Application of replaceable coupling beams to RC structures. *Structural Design of Tall & Special Buildings*, **25**(17):947-966. http://dx.doi.org/10.1002/tal.1292

Lv, X.L., Chen, Y., Mao, Y.J., 2011. New concept of structural seismic design: earthquake resilient structures. *Journal of Tongji University (Natural Science)*, **39**(7):941-948 (in Chinese).

Lv, X.L., Chen, C., Chen, Y., *et al*., 2016. Application of replaceable coupling beams to RC structures. *The Structural Design of Tall and Special Buildings*, **25**(17): 947-966. http://dx.doi.org/10.1002/tal.1292

Oh, S.H., Kim, Y.J., Ryu, H.S., 2009. Seismic performance of steel structures with slit dampers. *Engineering Structures*, **31**(9):1997-2008. http://dx.doi.org/10.1016/j.engstruct.2009.03.003

Plaud, J.J., Vogeltanz, N.D., 1997. Back to the future: the continued relevance of behavior theory to modern behavior therapy. *Behaviour Therapy*, **28**(3):403-414. http://dx.doi.org/10.1016/S0005-7894(97)80088-3

SAC (Standardization Administration of the People's Republic of China), 2003. Code for Design of Steel Structures, GB 50017-2003. SAC, Beijing, China (in Chinese).

SAC (Standardization Administration of the People's Republic of China), 2010. Metallic Materials–Tensile Testing at Ambient Temperature, GB/T228.1-2010. SAC, Beijing, China (in Chinese).

Wu, L., Chung, L., Tsai, S.F., *et al*., 2005. Seismic behavior of bolted beam-to-column connections for concrete filled steel tube. *Journal of Constructional Steel Research*, **61**(10):1387-1410. http://dx.doi.org/10.1016/j.jcsr.2005.03.007

Zhang, A.L., Zhang, Y.X., Liu, X.C., 2013. Research outlook of earthquake resilient prestressed steel structures. *Journal of Beijing University of Technology*, **39**(4):507-515 (in Chinese).

Zhang, A.L., Zhao, L., Liu, X.C., *et al*., 2014. Monotonic experimental study of prefabricated square tubular column to truss beam connections. *China Civil Engineering Journal*, **47**(S2):169-174 (in Chinese).

Zhang, A.L., Zhang, Y.X., Li, R., *et al*., 2016. Cyclic behaviour of a prefabricated self-centering beam-column connection with a bolted web friction device. *Engineering Structures*, **111**:185-198. http://dx.doi.org/10.1016/j.engstruct.2015.12.025

Zhang, A.L., Li, S.H., Jiang, Z.Q., *et al*., 2017. Design theory of earthquake-resilient prefabricated sinusoidal corrugated web beam-column joint. *Engineering Structures*, **150**:665-673. http://dx.doi.org/10.1016/j.engstruct.2017.07.088

Zhang, Y.X., Li, R., Wang, L.Y., *et al*., 2014. Study on seismic behaviour of strengthen-weaken beam-column connections in steel frames. *Progress in Steel Building Structures*, **16**(6):22-33 (in Chinese).

Zhou, X.H., Shi, Y., Zhou, T., *et al*., 2005. Cold-formed steel framing system of low-rise residential building. *Journal of Architecture and Civil Engineering*, **22**(02):5-18 (in Chinese).

中文概要

题　目：可恢复功能装配式梁柱中柱节点抗震性能研究

目　的：提出一种震后功能可快速恢复的装配式中柱节点，并建立其设计理论；考察装配式中柱节点的抗震性能及震后修复性能，并提出设计建议。

创新点：提出一种可快速恢复震后功能的装配式中柱节点；2. 提出装配式中柱节点设计理论，并通过数值手段对其合理性进行校核；3. 试验研究考察基础试件的抗震性能及震后修复性能。

方　法：1. 通过理论分析手段建立装配式中柱节点设计理论；2. 利用数值模拟手段通过 4 组 8 个算例来验证节点设计理论，并对节点抗震性能进行数值研究；3. 对基础试件进行低周往复荷载试验研究及修复试验研究，进一步验证设计理论的合理性，并考察节点的抗震性能及震后修复性能。

结　论：1. 提出的设计理论可准确地预测装配式中柱节点的屈服荷载；2. 设计合理的装配式中柱节点具有良好的承载性能及滞回特性，可满足结构震后功能修复要求；3. 翼缘连接盖板厚度和材性、中间螺栓间距和梁段间隙参数对节点抗震性能影响较大，需合理设置。

关键词：可恢复功能；翼缘盖板连接；狗骨削弱；设计理论；滞回性能